



HAL
open science

Metabolic Reprogramming in Amyotrophic Lateral Sclerosis

M. Szelechowski, N. Amoedo, E. Obre, Claire Léger, L. Allard, M. Bonneu, S. Claverol, Didier Lacombe, Stéphane Oliet, S. Chevallier, et al.

► **To cite this version:**

M. Szelechowski, N. Amoedo, E. Obre, Claire Léger, L. Allard, et al.. Metabolic Reprogramming in Amyotrophic Lateral Sclerosis. *Scientific Reports*, 2018, 8 (1), pp.3953. 10.1038/s41598-018-22318-5 . inserm-02647599

HAL Id: inserm-02647599

<https://inserm.hal.science/inserm-02647599>

Submitted on 29 May 2020

HAL is a multi-disciplinary open access archive for the deposit and dissemination of scientific research documents, whether they are published or not. The documents may come from teaching and research institutions in France or abroad, or from public or private research centers.

L'archive ouverte pluridisciplinaire **HAL**, est destinée au dépôt et à la diffusion de documents scientifiques de niveau recherche, publiés ou non, émanant des établissements d'enseignement et de recherche français ou étrangers, des laboratoires publics ou privés.

SCIENTIFIC REPORTS



OPEN

Metabolic Reprogramming in Amyotrophic Lateral Sclerosis

M. Szelechowski^{1,2}, N. Amoedo^{2,3}, E. Obre⁴, C. Léger^{1,2}, L. Allard^{1,2}, M. Bonneu^{5,2}, S. Claverol^{5,2}, D. Lacombe^{2,3}, S. Oliet^{1,2}, S. Chevallier^{1,2}, G. Le Masson^{1,2} & R. Rossignol^{2,3}

Received: 10 October 2017

Accepted: 21 February 2018

Published online: 02 March 2018

Mitochondrial dysfunction in the spinal cord is a hallmark of amyotrophic lateral sclerosis (ALS), but the neurometabolic alterations during early stages of the disease remain unknown. Here, we investigated the bioenergetic and proteomic changes in ALS mouse motor neurons and patients' skin fibroblasts. We first observed that SODG93A mice presymptomatic motor neurons display alterations in the coupling efficiency of oxidative phosphorylation, along with fragmentation of the mitochondrial network. The proteome of presymptomatic ALS mice motor neurons also revealed a peculiar metabolic signature with upregulation of most energy-transducing enzymes, including the fatty acid oxidation (FAO) and the ketogenic components HADHA and ACAT2, respectively. Accordingly, FAO inhibition altered cell viability specifically in ALS mice motor neurons, while uncoupling protein 2 (UCP2) inhibition recovered cellular ATP levels and mitochondrial network morphology. These findings suggest a novel hypothesis of ALS bioenergetics linking FAO and UCP2. Lastly, we provide a unique set of data comparing the molecular alterations found in human ALS patients' skin fibroblasts and SODG93A mouse motor neurons, revealing conserved changes in protein translation, folding and assembly, tRNA aminoacylation and cell adhesion processes.

Amyotrophic lateral sclerosis (ALS) is a rapidly progressive neurological disease characterized by the gradual degeneration and death of motor neurons, followed by global muscle wasting. Brain and systemic hypermetabolism have been observed in ALS patients, suggesting that energy-wasting mechanisms contribute to either ALS pathogenesis or adaptation to the disease. Numerous studies have investigated oxidative phosphorylation (OXPHOS) in different ALS models and revealed a global inhibition of the mitochondrial respiratory chain^{1–5}. However, this does not explain energy wasting that rather suggests a defective coupling between mitochondrial respiration and ADP phosphorylation^{6,7} and/or a stimulation of the central metabolism and energy-transducing pathways. Uncoupling protein 2 (UCP2) was previously found to participate in mitochondrial reprogramming in ALS⁸. However, further bioenergetic and biochemical analyses showed that UCP2 does not uncouple OXPHOS as expected^{8–14} but rather accommodates a metabolic shift from glucose to fatty acid oxidation (FAO)¹⁵ and induce ketone body formation by exporting C4 metabolites as oxaloacetate out of mitochondria¹⁶. In line with this view, a metabolic shift toward FAO and ketogenesis was observed in the skeletal muscle of ALS patients¹⁷ and a genetic mouse model⁴, and UCP2 expression itself was shown to depend upon the activation of fatty acid metabolism¹⁸. Still, the bioenergetic and proteomic profiles of ALS presymptomatic motor neurons remain unknown, and the relative expression of glycolytic, OXPHOS and FAO enzymes has been underinvestigated. In conditions of hypermetabolism as it was extensively described in ALS, the mitochondrial respiratory chain require the sustained fueling of energy substrates to maintain a minimal electric membrane potential ($\Delta\psi$) to avoid both a REDOX crisis and activation of apoptosis¹⁹. Given its higher yield in reductive equivalents compared with glucose oxidation, FAO could fulfill this requirement¹⁵. Moreover, in SOD1-related ALS cases or models, misfolded mutant SOD1 protein binds to and inhibit VDAC conductance at the mitochondrial outer membrane, thereby inducing bioenergetic blockade². As fatty acids can diffuse through the mitochondrial outer membrane, FAO could by-pass this bioenergetic blockade. On the other hand, a long-term and chronic higher reliance on FAO could be toxic since FAO generates ketone bodies and ketoacidosis was shown to alter neurons viability in other metabolic pathologies such as in maple syrup urine disease and 2-methyl-3-hydroxybutyryl-CoA dehydrogenase deficiency.

¹INSERM U1215, Neurocentre Magendie, 33077, Bordeaux, cedex, France. ²Bordeaux University, 33000, Bordeaux, France. ³INSERM U1211, MRGM, 33000, Bordeaux, France. ⁴CELLOMET, Center of Functional Genomics (CGFB), 146 Rue Léo Saignat, 33000, Bordeaux, France. ⁵Center of Functional Genomics (CGFB), Proteomic Facility, Bordeaux University, 33000, Bordeaux, France. M. Szelechowski, N. Amoedo and E. Obre contributed equally to this work. G. Le Masson and R. Rossignol jointly supervised this work. Correspondence and requests for materials should be addressed to G.L.M. (email: gwendal.lemasson@inserm.fr) or R.R. (email: rodrigue.rossignol@u-bordeaux.fr)

Therefore, more detailed knowledge of the bioenergetics and proteome remodeling of presymptomatic motor neurons is required to derive adapted nutritional and pharmacological therapeutic strategies in ALS. Several lines of evidence indicate that motor neurons require OXPHOS^{20–22} for survival, and pro-OXPHOS protective metabolic approaches have been considered in clinical nutritional studies²³. Recent studies have also revealed that during neuronal differentiation, the activation of OXPHOS is a critical checkpoint, and alterations in metabolic reprogramming impact neuronal survival^{24–26}. However, the design of therapeutic approaches adapted to ALS neurometabolic specificities is hampered by our limited knowledge of motor neuron bioenergetics and metabolic reprogramming in ALS pathology. For instance, a systemic ketogenic diet could be deleterious if ALS motor neurons are already challenged, at the cellular level, by ketoacidosis secondary to adaptive FAO. While metabolic remodeling has been extensively described in cancer, diabetes, mitochondrial diseases and autoimmune disorders (for review see²⁷), little information is available about this topic in neurodegenerative diseases such as ALS²⁸. In the present study, we analyzed the bioenergetic alterations and the molecular changes in ALS mice motor neurons and patients' skin fibroblasts. Our results unraveled the specificities of metabolic remodeling in ALS mouse motor neurons and patients' skin fibroblasts.

Results

Bioenergetic alterations in presymptomatic SODG93A (ALS) mouse motor neurons. To gather a better understanding of the metabolic changes in presymptomatic ALS mice motor neurons, we performed a detailed bioenergetic and metabolic pathway proteome reprogramming analysis as summarized in Fig. 1A. First, respiration showed lower values in SODG93A mutant mice motor neurons than in wild-type ones under routine and FCCP (maximal respiration) conditions (Fig. 1B), as defined in the methods. A lower coupling degree of OXPHOS was also measured in ALS motor neurons, as determined by the reduced Routine/Oligo ratio (see methods). Accordingly, both the total cellular and the mitochondrial steady-state ATP levels were reduced in ALS motor neurons (Fig. 1C). The observed reduction in routine respiration was in agreement with the observed decrease in mitochondrial transmembrane electric potential ($\Delta\psi$) measured in these conditions (Fig. 1D,E). The altered OXPHOS coupling in SODG93A mice motor neurons was not explained by usual uncoupling since routine respiration was not higher than in the wild-type mice motor neurons, and since respiration could be chemically uncoupled with Carbonyl cyanide-4-(trifluoromethoxy)phenylhydrazone (FCCP) (Fig. 1B). The FCCP/Routine ratio was even higher in SODG93A (ALS) motor neurons than in wild-type cells, indicating a large excess capacity of oxidative phosphorylation (Fig. 1B).

Therefore, our findings on ALS presymptomatic mouse motor neurons revealed *i*) an inhibition of mitochondrial respiration, *ii*) a reduction of OXPHOS coupling, *iii*) the non-occurrence of a pre-existing disease-related uncoupling, and *iv*) a lower steady-state mitochondrial electric transmembrane potential and cellular ATP level. Mitochondrial $\Delta\psi$ participates in the maintenance of organelle morphogenesis²⁹, and significant alteration of the mitochondrial network was observed in motor neurons from ALS mice (Fig. 1F–H). In particular, a reduction in mitochondrial tubule size was observed, in agreement with the dependency of mitochondrial fusion on $\Delta\psi$ ³⁰. The mitochondrial network total area per motor neuron (mitochondrial density) was obtained as the ratio of the area of the TOM20 labeling to that of the SMI32 labeling. The data (Fig. 1H) indicated no significant difference in this parameter between WT and the ALS presymptomatic mouse motor neurons. Altogether, the investigation of mitochondrial physiology in ALS mice motor neurons revealed the occurrence of mitochondrial bioenergetic deficiencies and alterations in mitochondrial network architecture.

UCP2 inhibition in ALS motor neurons alters bioenergetics but does not impact the redox status. Previous investigations linked the uncoupling protein 2 (UCP2) to mitochondrial dysfunction in ALS^{31,32}, so we tested the role of this protein in the bioenergetic alterations of ALS mice motor neurons observed in our study. Pharmacologic UCP2 inhibition with genipin induced a significant increase in the cellular ATP level (Fig. 2A) in ALS mice motor neurons and recovered the normal morphology of the mitochondrial network (Fig. 2B). However, no change in H₂O₂ level or ROS-scavenging capacity was triggered by genipin in both ALS and wild-type mice motor neurons in our experimental conditions (Fig. 2C). Likewise, the redox state of glutathione was not altered by UCP2 inhibition (Fig. 2D). Therefore, no direct sign of oxidative stress was found in presymptomatic ALS motor neurons, as neither the steady state level of H₂O₂ nor the GSH redox state showed differences between SODG93A and WT cells (Fig. 2C and D). However, a significant increase in antioxidant defense systems (SOD2 and catalase) was measured in the SODG93A motor neurons by western blot (Fig. 2E–I), suggesting an indirect sign of oxidative stress. These findings indicate that in ALS motor neurons, UCP2 participates in ATP synthesis as recently proposed¹⁶ and not act as an uncoupling protein.

Proteome remodeling in presymptomatic motor neurons from ALS mice. To investigate the broad impact of the SODG93A mutation in mice motor neurons, we performed a large-scale molecular study using label-free proteomics. Firstly, we evaluated the cellular functions (Gene Ontology term (GO terms)) over-represented in the differential proteomic dataset. The results indicated that energy-transducing enzymes belonging to several pathways such as FAO, the TCA cycle, glycolysis and OXPHOS were increased (Fig. 3A). In addition, different functions linked with protein translation, folding or complex assembly were also over-represented. Likewise, over-representation of proteins implicated in mRNA splicing, chromosome segregation and chromatin organization was observed in presymptomatic ALS mouse motor neurons.

Secondly, we compared the proteome of SODG93A and WT mouse motor neurons. This analysis identified 496 proteins that differed in content between the two groups of motor neurons (ALS vs WT, $p < 0.05$). A total of 290 proteins were over-represented in ALS (fold change ranging from 1.12 to >1000), and 206 were repressed. A global analysis of the cellular functions impacted by those changes, taking into account both the over- or under-expressed proteins with a cut-off of $-\text{Log}(p \text{ value}) > 2.5$, was performed using Ingenuity Pathway Analysis

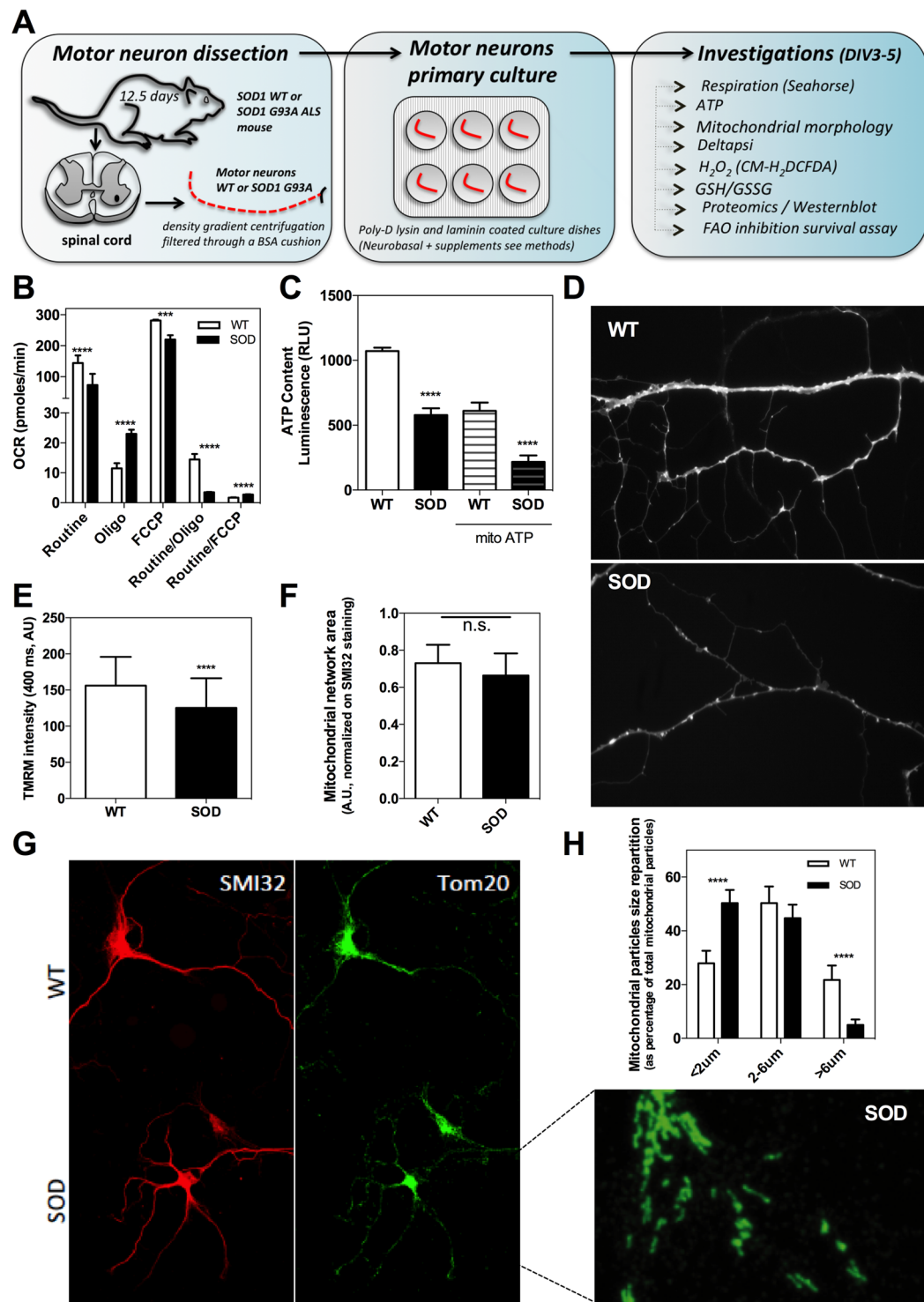


Figure 1. Bioenergetics of SOD1G93A ALS motor neurons. (A) Schematic workflow of the biochemical and cell biology investigations on presymptomatic mouse motor neurons at DIV3-5. (B) Oxygen consumption rate (OCR determined on the Seahorse XF96 extracellular flux analyzer) on SOD1G93A ALS mouse motor neurons (SOD) or wild-type mouse motor neurons (WT). Mitochondrial respiration was measured in routine, oligo or FCCP conditions as explained in the methods. (C) Total and mitochondrial steady-state ATP content in SOD or WT motor neurons. (D) Representative image of the TMRM signal for the measurement of mitochondrial transmembrane electric potential ($\Delta\psi$) in WT or SOD mice motor neurons and (E) related quantification. (F) Mitochondrial network total area (TOM20 labelling) in mouse motor neurons normalized to the cellular area (SMI32 labeling) and corresponding images (G). (H) Mitochondrial network morphometric analysis in mouse motor neurons.

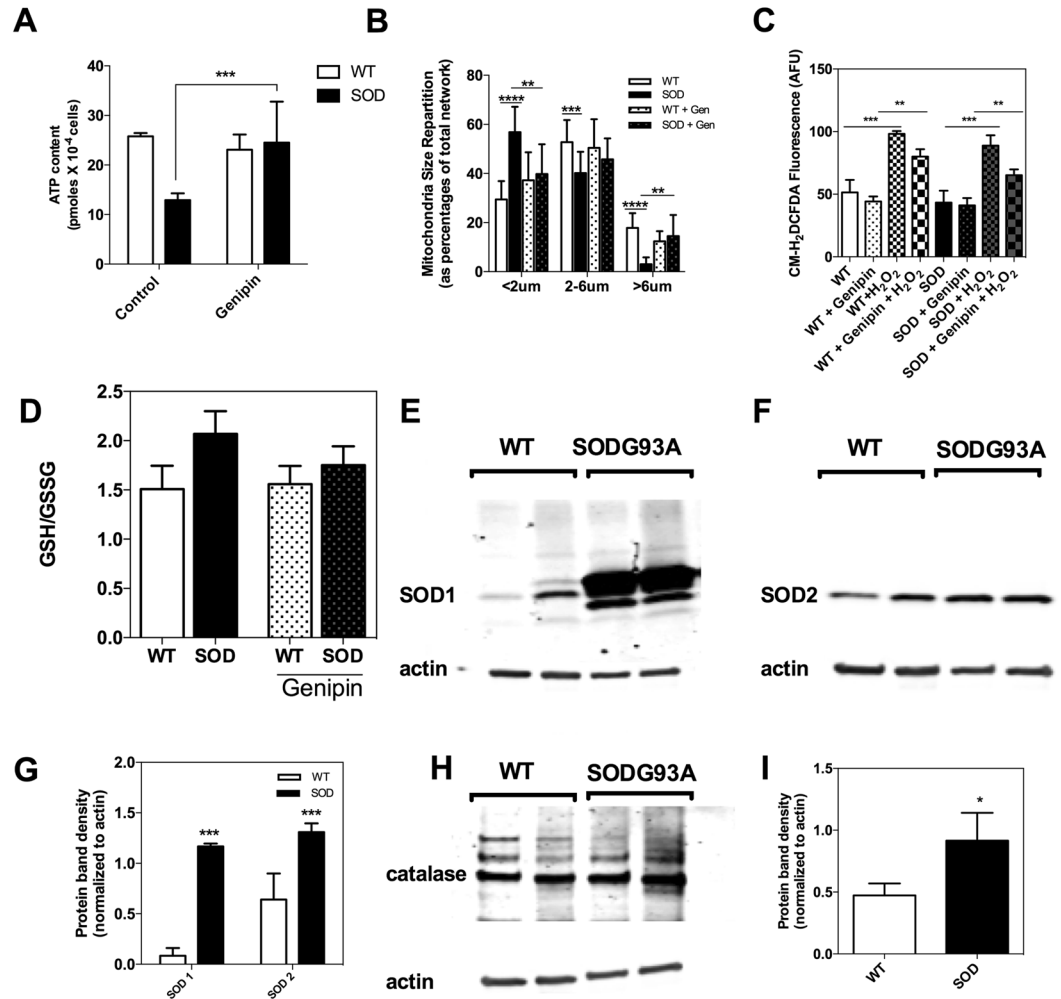


Figure 2. Role of UCP2 in ALS motor neurons bioenergetics and H_2O_2 -scavenging. (A) Effect of UCP2 inhibition with genipin on motor neurons total ATP level, (B) mitochondrial network morphology, (C) H_2O_2 steady-state level (as measured by CM- H_2DCFDA fluorescence) and (D) glutathione redox state. (E) Westernblot analysis of the expression level of SOD1, (F) SOD2 and (G) relative quantification of SOD1 and SOD2 protein content (normalized to actin). (H) Westernblot analysis of the expression level of catalase and (I) relative quantification of catalase protein content (normalized to actin).

(IPA, Fig. 3B). The top five IPA pathways that differ between ALS and WT motor neurons were ‘EIF2 signaling ($p = 2.61 \text{ E-}14$)’, ‘TCA cycle ($p = 2.14 \text{ E-}13$)’, ‘mitochondrial (dys)function ($p = 2.11 \text{ E-}11$)’, ‘oxidative phosphorylation ($p = 2.29 \text{ E-}8$)’ and ‘tRNA charging ($p = 1.15 \text{ E-}6$)’. Of note, the ‘superpathway of cholesterol biosynthesis (via mevalonate)’ was also upregulated in SOD motor neurons with $-\log p = 2.82$.

The top two protein networks significantly different between ALS and WT mouse motor neurons (Supplemental Figure S1A and B, respectively) were ‘protein synthesis, protein degradation cellular assembly and organization’ (score 38) and ‘lipid metabolism, small molecule biochemistry, energy production’ (score 28). The search for predicted regulators of the observed proteomic differences in ALS *versus* WT motor neurons identified 4 inhibited factors ($p < 0.05$) and 8 activated ones (Fig. 3C). The proteome analysis also suggested that neuritogenesis and formation of cellular protrusions could be activated in ALS mice motor neurons based on the increased expression of specific proteins involved in these functions (Supplemental Table S1). The predicted alteration (activation Z score > 2 or < -2) of other cellular functions as ‘cell death’, ‘organization of the cytoskeleton’, ‘microtubule dynamics’, ‘fragmentation of DNA’ and ‘concentration of fatty acids’ was also detected in this analysis (Supplemental Table S1). Altogether, the proteomic survey indicated an important modification of the metabolic machinery in motor neurons from ALS mice, with a particular enhancement of the molecular systems involved in oxidative energy metabolism. The Kyoto Encyclopedia of Genes and Genomes (KEGG) pathway analysis of the proteins over-represented in the ALS motor neuron proteome provided a more detailed description of the changes in the canonical metabolic pathways (Supplemental Table S2). It showed a large number of differences ($\text{FDR} < 0.05$) in energy-transducing pathways such as OXPHOS, TCA cycle, branched-chain amino-acids degradation, propanoate metabolism, glycolysis and fatty acid oxidation. A metabolic chart of those changes is shown in Fig. 4, demonstrating the major differences in the mitochondria, with a dramatic increase in ACAT2

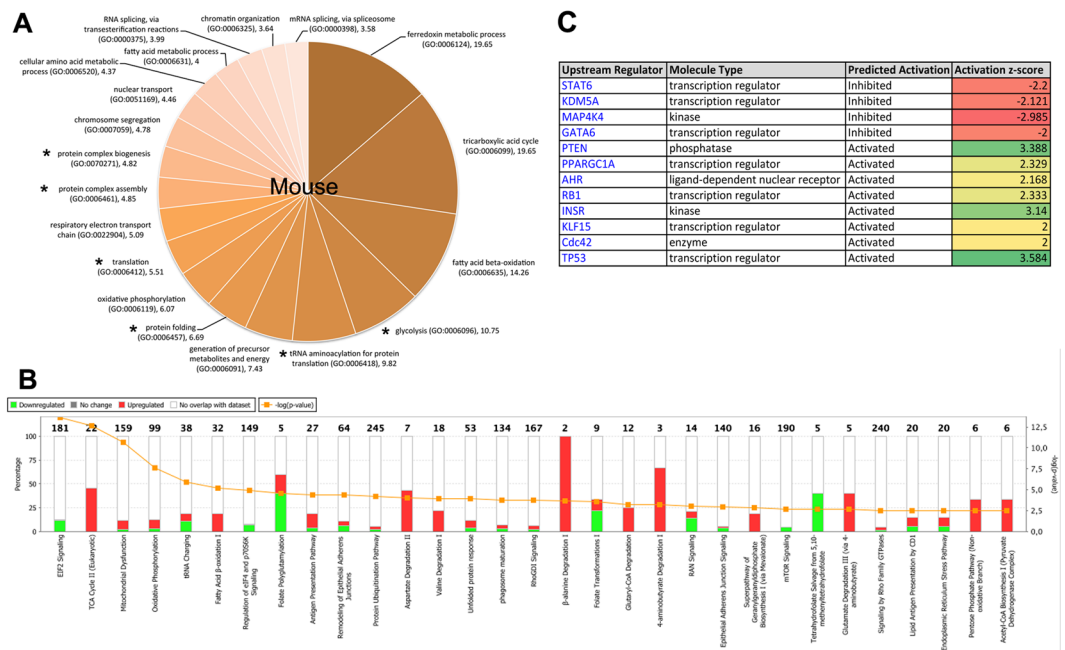


Figure 3. SODG93A ALS mouse motor neurons proteome. **(A)** Over-represented GO terms in the proteome of ALS mouse motor neurons as compared to the mouse reference transcriptome. **(B)** Comparison of the proteome of SODG93A ALS mice motor neurons and that of wild-type mice motor neurons. The Ingenuity Pathways Analysis was performed to identify the pathway significantly different ($p < 0.05$) between the two proteomes. The $-\log p$ value is shown in the orange line and in the bottom abscissa. The percentage of proteins from the pathway found in the differential proteome is given in the top abscissa. **(C)** Table of the predicted main regulators of the ALS mouse motor neurons proteome remodeling.

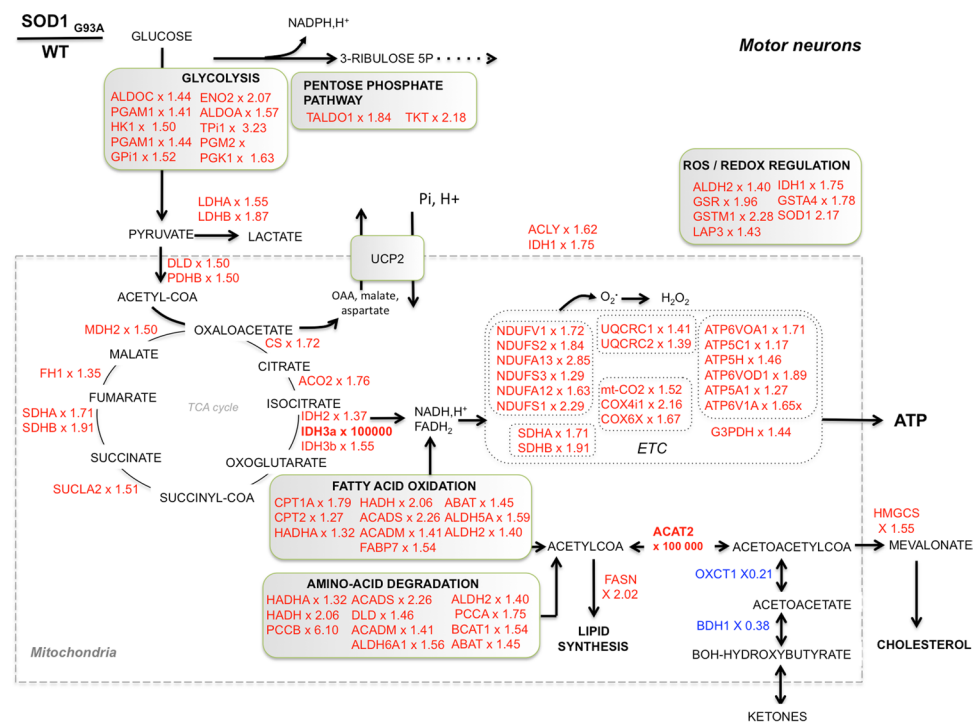


Figure 4. Proteome remodeling in SODG93A ALS motor neurons. Chart of the metabolic proteome remodeling in SODG93A ALS motor neurons. Over represented proteins appear in red and the corresponding fold change (SOD/WT) is given after the name of each protein.

Decreased proteostasis components in ALS
RS2_HUMAN, RS3_HUMAN , RS3A_HUMAN, RS4X_HUMAN, RS4Y1_HUMAN, RS4Y2_HUMAN, RS5_HUMAN, RS6_HUMAN, RS7_HUMAN, RS8_HUMAN, RS9_HUMAN, RS10_HUMAN, RS11_HUMAN, RS12_HUMAN, RS13_HUMAN, RS14_HUMAN , RS15_HUMAN, RS15A_HUMAN, RS16_HUMAN, RS17_HUMAN, RS18_HUMAN, RS19_HUMAN, RS20_HUMAN, RS21_HUMAN, RS23_HUMAN , RS24_HUMAN, RS25_HUMAN, RS26_HUMAN, RS27_HUMAN, RS28_HUMAN, RS29_HUMAN, RS30_HUMAN, RSSA_HUMAN, Gm6336, Gm2000, Gm6139, SBDS, RAN, Gtpbp4, RL3_HUMAN, RL4_HUMAN, <i>RL5_HUMAN</i> , RL6_HUMAN, <i>RL7A_HUMAN</i> , RL7_HUMAN, RL8_HUMAN , RL9_HUMAN, RL10A_HUMAN, RL11_HUMAN , RL12_HUMAN, RL13A_HUMAN, RL14_HUMAN, RL15_HUMAN, RL17_HUMAN, RL18A_HUMAN, RL19_HUMAN, RL21_HUMAN, RL22_HUMAN, RL23A_HUMAN, <i>RL23_HUMAN</i> , RL24_HUMAN, RL26_HUMAN, RL27A_HUMAN, RL27_HUMAN, RL28_HUMAN, RL29_HUMAN, RL30_HUMAN, RL31_HUMAN, RL32_HUMAN, RL34_HUMAN, RL35A_HUMAN, RL35_HUMAN, RL36A_HUMAN, RL36_HUMAN, RL37A_HUMAN, RL37_HUMAN, RL38_HUMAN, RL39_HUMAN, RL40_HUMAN, RL41_HUMAN, RLA0_HUMAN, RLA1_HUMAN, RLA2_HUMAN.
Increased proteostasis components in ALS
CANX, HSPA5 , MOGS, HYOU1, PRKCSH, CKAP4, DDOST , UGGT1, PDIA3 , CALR, RPLP1, RPL24, RPS8, Capn2, Vcp, Hspa5 , Lman2, Ddost , Pdia3 , Ganab, <i>Pdia4</i> , <i>Calr</i> , <i>Rpl19</i> .

Table 1. Detail of the proteomic changes in ribosomal subunits and in components of the protein processing in the ER system in ALS mice motor neurons and ALS patients skin fibroblasts. This table was obtained from the Kyoto Encyclopedia of Genes and Genomes (KEGG) analysis of the proteomic datasets obtained on ALS mouse motor neurons and in ALS patient's skin fibroblasts. The subunits altered in skin only are written in italic, the subunit altered in motor neurons only are in normal case and all the ones altered in both skin and motor neurons are in bold.

(ketone metabolism). In addition to energy metabolism, lysosome, phagosome and protein processing in the ER were also observed among the over-represented KEGG pathways in ALS mice motor neurons (Supplemental Table S2). Lastly, the KEGG analysis of the proteins under-represented in ALS mice motor neurons (Supplemental Table S3) showed a significant (FDR < 0.05) alteration of the 'ribosomes', 'spliceosome' and components belonging to the 'protein processing in endoplasmic reticulum' category. A detailed analysis of the changes in ribosomal proteins is shown in Table 1. Two proteins involved in the synthesis and degradation of ketone bodies were also identified in the under-represented KEGG pathways, namely 3-hydroxybutyrate dehydrogenase 1 (BDH1) and 3-oxoacid-CoA transferase 1 (OXCT1). Lastly, the KEGG analysis of the under-represented pathways in ALS mice motor neurons (Supplemental Table S3) identified gap junction, focal adhesion and tight junction, suggesting a possible alteration of the cell adhesion processes of motor neurons.

OXPHOS decoupling and proteome remodeling in skin fibroblasts from ALS patients. Similar to mice motor neurons, we compared mitochondrial bioenergetics and proteome composition in human skin fibroblasts taken from ALS patients (Supplemental Table S4) with controls (male 58 years old and female 46 years old). Respiration analysis first showed a reduced OXPHOS coupling, as assessed by a reduced effect of oligomycin, without changes in routine respiration (Fig. 5A). This reduction in OXPHOS coupling was associated with a corresponding decrease in the steady-state ATP level and an increase in ADP content in ALS patients' skin fibroblasts (Fig. 5A). The uncoupling ratio (FCCP-stimulated respiration/oligomycin-treated respiration) was also reduced in the patient's fibroblasts as compared to the controls (Fig. 5A).

The over-representation test performed on the proteome of ALS skin fibroblasts (Fig. 5B) showed enrichment in the altered expression of proteins of glycolysis, translation, protein folding, protein complex biogenesis, protein complex assembly, and tRNA aminoacylation. To better analyze the proteome specificities of ALS human skin fibroblasts, we performed a comparison with skin fibroblasts obtained from age-matched healthy individuals. This comparison identified 115 over-represented and 262 under-represented proteins in ALS skin fibroblasts. The Ingenuity Pathway Analysis (Fig. 5C) indicated major changes in 'EIF2 signaling', 'TCA cycle', 'oxidative phosphorylation', 'fatty-acid oxidation', 'remodeling of epithelial adherens junctions', and 'glycolysis' (see complete list in Table S5). A more detailed search for the alterations in cellular metabolic pathways (using the 'toxicology' module of IPA) showed modification of 'fatty acid metabolism', 'NRF2-mediated oxidative stress response' and 'PPAR α /RXR α pathway activation ($p < 0.05$). The main predicted regulators of the observed proteomic changes are listed in Supplemental Table S6. In particular, IPA predicted the activation of three transcription factors (TFAP2A, JUNB, and PDX1) and the inhibition of five others (HSF1 and HSF2 involved in the proteotoxic stress response, NFE2L2 involved in the antioxidant response and, MYCN and MYC involved in cellular reprogramming). Regarding MYC, 85 targets of this transcription factor were found in the difference proteome (Supplemental Figure S2). Activation of the mTORC2 central component RICTOR was also predicted by IPA (32 target genes; Supplemental Figure S2).

The KEGG analysis of the proteins over-represented (FDR < 0.05) in ALS patients' skin fibroblasts revealed enrichment in 'protein processing in endoplasmic reticulum', 'focal adhesion' and 'tight junctions' (Table 2). Concerning the changes in metabolic pathways, the two subunits of the mitochondrial trifunctional protein complex (HADHA and HADHB) involved in fatty acid oxidation were overexpressed. Another related major change in ALS mice motor neurons was the expression of ACAT2, a protein involved in the reversible production of ketones from the main FAO final product: acetyl-coA. Lastly, the analysis of the proteins under-represented in the ALS patients' skin fibroblasts revealed a significant (FDR < 0.05) reduction in components of glycolysis, ribosome, focal adhesion, proteasome, RNA transport, fatty-acids degradation and pentose phosphate pathway (Table S7).

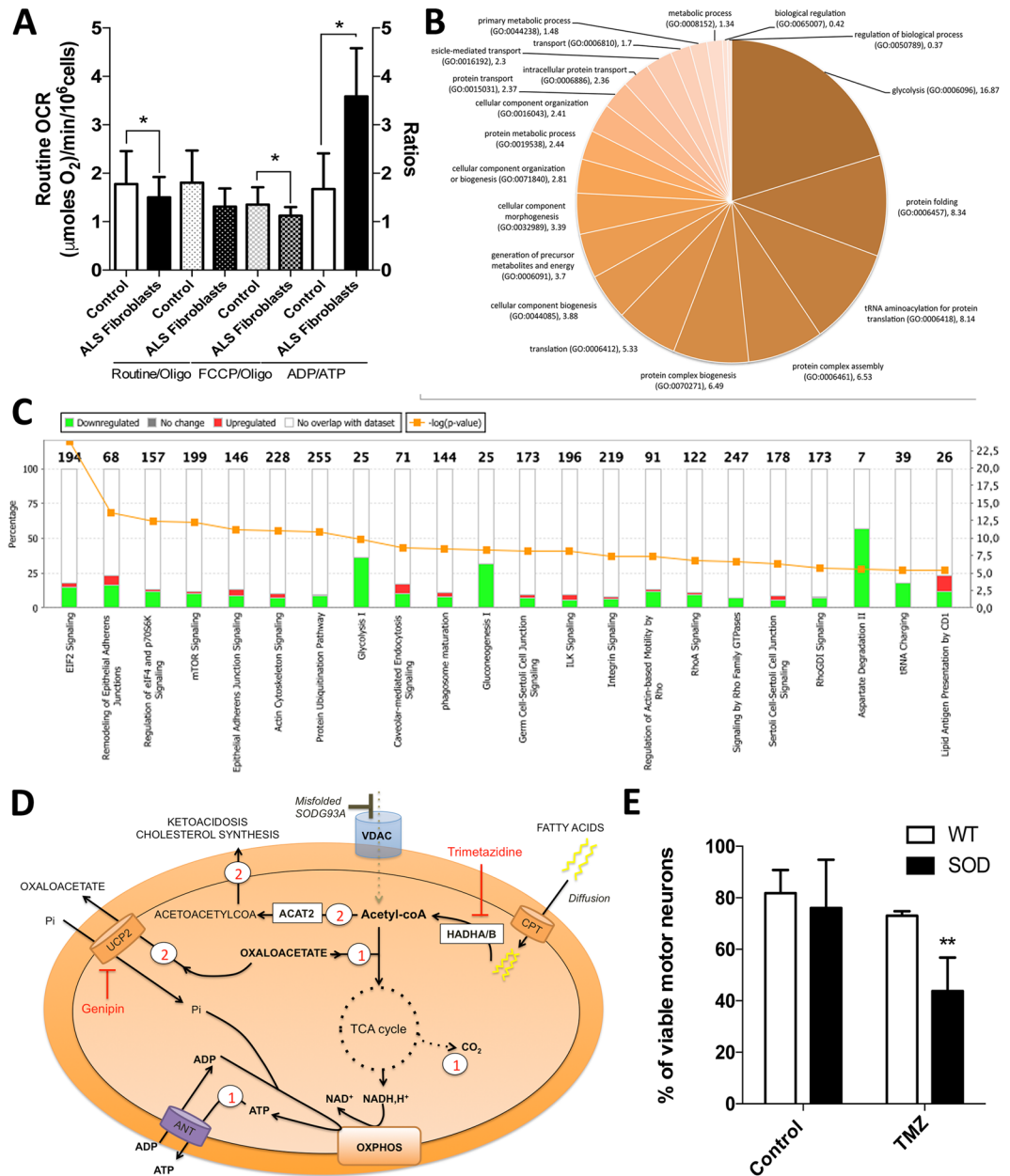


Figure 5. Bioenergetic alterations and proteome remodeling in ALS patient skin fibroblasts. **(A)** Respiration of skin fibroblasts in routine conditions and calculation of the respiratory control ratio (routine/oligo respiration) and of the uncoupling ration (FCCCP/oligomycin respiration). **(B)** ADP/ATP ratio determined in skin fibroblasts. **(C)** Proteome analysis (over-representation test) of ALS skin patients fibroblasts. **(D)** Comparison of the proteome between ALS skin patients fibroblasts and fibroblasts from healthy individuals. Ingenuity Pathway Analysis (IPA) was performed and the pathway with a difference of $-\log p$ value > 5 are shown. **(E)** Bioenergetic model of ALS adaptive metabolism showing the role of HADHA, ACAT2, UCP2 and HMGCS1. In this hypothetical model, ALS motor neurons shift to FAO and amino-acids degradation to transduce energy but in turn generate acetyl-CoA which can then be used for fatty-acid synthesis, ketogenesis and cholesterol synthesis. Therefore, a fine tuning between the use of FAO and the elimination of acetyl-CoA must be maintained to promote cell survival, and UCP2 could play a central role in this balance. In our model, the use of acetyl-coA produced by FAO for either oxidative phosphorylation (route 1) or ketogenesis and cholesterol synthesis (route 2) depends on the export of oxaloacetate by UCP2 (route 2), as proposed by Vozza *et al.*¹⁶. In line with this hypothesis, (i) the inhibition of UCP2 with genipin leads to an increase in cellular ATP levels (blockade of route 1; Fig. 2A), while ii) the blockade of FAO using trimetazidine (HADHB inhibitor) reduces cell viability in SOD motor neurons (blockade of route 1), with minor effects on wild-type cells (Fig. 5E). This model considers previous findings indicating that VDAC is blocked by mutant-SOD in ALS², forcing cells to depend on outer membrane-diffusive energy sources such as fatty acids. It also considers recent findings showing the accumulation of cholesterol in the cerebrospinal fluid of ALS patients³³.

Pathway description	FDR	Overexpressed proteins in ALS patient's fibroblasts
Protein processing in endoplasmic reticulum	6.89E-08	CALR,CANX,CKAP4,DDOST,HSPA5,HYOU1,MOGS,PDIA3,PDIA4,PRKCSH,UGGT1
Amoebiasis	7.86E-05	ACTN1,ACTN4,COL1A2,COL5A1,FN1,GNAQ,RAB7A
Focal adhesion	0.000439	ACTN1,ACTN4,COL1A2,COL5A1,FLNA,FLNB,FN1,ITGAV
Thyroid hormone synthesis	0.00133	CANX,GNAQ,GPX8,HSPA5,PDIA4
Salmonella infection	0.00216	FLNA,FLNB,MYH10,MYH9,RAB7A
Regulation of actin cytoskeleton	0.00252	ACTN1,ACTN4,FN1,GSN,ITGAV,MYH10,MYH9
Antigen processing and presentation	0.0103	CALR,CANX,HSPA5,PDIA3
Tight junction	0.0113	ACTN1,ACTN4,CTNNA1,MYH10,MYH9
Arrhythmogenic right ventricular cardiomyopathy	0.0119	ACTN1,ACTN4,CTNNA1,ITGAV
ECM-receptor interaction	0.0173	COL1A2,COL5A1,FN1,ITGAV
Protein digestion and absorption	0.0173	COL12A1,COL1A2,COL5A1,SLC3A2
Lysine degradation	0.0388	GLT25D1,HADHA,PLOD3

Table 2. Kyoto Encyclopedia of Genes and Genomes (KEGG) pathway analysis of the over- and under-expressed components in ALS ($P < 0.05$; at least 2 proteins per pathway). FDR (False discovery Rate).

ALS motor neuron survival relies on FAO. The proteomic analyses described above indicated that several components of the fatty-acids oxidation system were upregulated both in ALS mouse motor neurons and ALS patients' skin fibroblasts. Conversely, the ketone bodies metabolizing enzymes BDH1 and OXCT1 were repressed while ACAT2 was strongly upregulated as well as the cytoplasmic hydroxymethylglutaryl-CoA synthase involved in cholesterol synthesis 1 (see Fig. 4). Moreover, we found that UCP2 activity was linked with energy homeostasis in ALS motor neurons (Fig. 2A), which is consistent with UCP2 role in exporting oxaloacetate from mitochondria. Lastly, the biochemical survey of lipid metabolism performed in ALS patients indicated ketonuria in three out of the five patients investigated (Supplemental Table S4). Taken together, these proteomic and bioenergetic findings could suggest a working model of ALS motor neurons metabolic rewiring as illustrated in Fig. 5D. In this hypothetical model, ALS motor neurons shift to FAO and amino acids degradation to transduce energy but in turn generate acetyl-CoA, which can then be used for fatty-acid synthesis, ketogenesis and cholesterol synthesis. Therefore, a fine tuning between the use of FAO and the elimination of acetyl-CoA must be maintained to promote cell survival, and UCP2 could play a central role in this balance. In our model, the use of acetyl-coA produced by FAO for either oxidative phosphorylation (route 1) or ketogenesis and cholesterol synthesis (route 2) depends on the export of oxaloacetate by UCP2, as proposed by Voza *et al.*¹⁶. In line with this hypothesis, (i) the inhibition of UCP2 with genipin leads to an increase in cellular ATP levels (blockade of route 1; Fig. 2A), while ii) the blockade of FAO using trimetazidine (HADHB inhibitor) reduces cell viability in SOD motor neurons (blockade of route 1), with minor effects on wild-type cells (Fig. 5E). This model considers previous findings indicating that VDAC is blocked by mutant-SOD in ALS², forcing cells to depend on mitochondrial outer membrane-diffusive energy sources such as fatty acids. It is also consistent with recent observations of cholesterol accumulation in the cerebrospinal fluid of ALS patients³³.

Discussion

Alteration of energy metabolism is considered to be a hallmark of amyotrophic lateral sclerosis pathophysiology³⁴ since multiple lines of evidence have shown inhibition of respiratory chain enzymes complex activity in patients' muscle³⁵ and spinal cord³⁶ samples, as well as in tissues of ALS mice models^{37,38}. Still, little is known about the bioenergetics and proteomic changes in ALS motor neurons during the early stages of the disease.

In the present study, we analyzed the bioenergetics and molecular reprogramming of embryonic presymptomatic motor neurons from SODG93A ALS mice at 2 to 5 DIV. We found a defective oxidative phosphorylation system, characterized by reduced respiration and lower coupling, which accentuates ATP depletion. The inhibition of the respiratory chain system was previously explained by the blockade of VDAC by the misfolded mutated form of SOD1², and the altered OXPHOS coupling was thought to result from the perturbation of mitochondrial structure³⁹. Accordingly, we observed an increased fragmentation of the mitochondrial network in ALS mice motor neurons, as well as a reduced mitochondrial transmembrane electric potential. This is totally consistent with the dependency of mitochondrial morphology and dynamics on mitochondrial bioenergetics²⁹ and on transmembrane electric potential³⁰. Our findings demonstrate that oxidative phosphorylation is not uncoupled in ALS but rather decoupled since the ADP-stimulated rate of respiration was reduced (lower effect of oligomycin) while the non-phosphorylating respiratory rate was not increased and was sensitive to the effect of uncouplers. The difference and theoretical background between uncoupling and decoupling was extensively discussed by Rottenberg H.⁴⁰ Briefly, OXPHOS uncoupling is characterized by a reduced mitochondrial transmembrane electrochemical gradient of protons associated with an increased proton permeability and reduced respiratory rate, while decoupling is characterized by a reduction of the ADP-stimulated rate of respiration without increase in non-phosphorylating rate of respiration.

Our molecular investigations revealed that ALS mutant motor neurons, with defective bioenergetics, have developed adaptive strategies to survive. Indeed, using comprehensive label-free proteomics, we found that most pathways involved in glucose, fatty-acid, and amino acid catabolism are up-regulated in ALS mice motor neurons, while only amino-acid degradation pathways and a step of fatty-acid oxidation are enhanced in patients' skin fibroblasts. In particular, our study revealed a potential biomarker that is increased in both ALS mice motor neurons and patients' skin fibroblasts: HADHA, the trifunctional enzyme complex subunit alpha located in the mitochondria, also known as hydroxyacyl-CoA dehydrogenase/3-ketoacyl-CoA thiolase/enoyl-CoA hydratase. Validation of this potential biomarker will require investigation in a larger group of ALS patient samples as recently performed for the urinary extracellular domain of the neurotrophin receptor p75-ECD⁴¹.

While numerous studies have indicated that neuronal bioenergetics depends primarily on glucose catabolism via the neuron-glia metabolic symbiosis, an NMR study performed in adult rat brain showed that approximately 20% of the total energy was obtained from fatty acids⁴². Our findings demonstrated that ALS mice motor neurons rely directly on this pathway for survival. More generally, enhanced expression of β -oxidation enzymes features a bioenergetic adaptive process in situations of metabolic stress⁴³, as it was already proposed in idiopathic Parkinson's disease⁴⁴. Still, FAO generates toxic end-products as ketone bodies, and a bioenergetic shift toward FAO could have implications for neuron viability if ketoacidosis occurred. Accordingly, another protein strongly over-represented in ALS mice motor neurons was acetyl-CoA acetyltransferase 2 (ACAT2), which catalyzes the reversible conversion of two units of acetyl-CoA to acetoacetyl CoA (ketogenesis) or the thiolytic cleavage of 3-ketoacyl-CoA into two-carbon chain-shortened acyl-CoA plus acetyl-CoA (ketosis). In the context of an increased expression of fatty-acid oxidation enzymes (notably the mitochondrial trifunctional protein), ACAT2 over-expression may facilitate the removal of the FAO end-product acetyl-coA, to produce acetoacetyl CoA. Given that ALS motor neurons display a strongly reduced expression of two enzymes involved in ketone bodies formation and utilization, namely 3-hydroxybutyrate dehydrogenase 1 (BDH1) and 3-oxoacid-CoA transferase 1 (OXCT1), one could hypothesize that the acetoacetyl-CoA could be used for cholesterol synthesis by the mevalonate pathway. This view is supported by the increased expression of the HMG-CoA-Synthase 1 that we observed in ALS mouse motor neurons (see Fig. 4) and the recent discovery of increased levels of cholesterol in the CSF of ALS patients³³. However, we cannot exclude a role of ACAT2 in ketosis and OXPHOS fueling, and this point will require further metabolic investigations.

We did not find any evidence of downregulation of respiratory chain subunits in the proteome of ALS skin fibroblasts but we discovered a downregulation of glucose metabolism (glycolysis) and malate-aspartate shuttle components (GOT1, GOT2, MDH2) suggesting a reduced fueling of OXPHOS rather than a decreased biogenesis of the respiratory chain. Conversely, the proteome of ALS motor-neurons showed a strong increase in the expression of respiratory chain proteins indicative of a compensatory response to the initial OXPHOS defect secondary to SOD1 mutation, as proposed by Israelson, A *et al.*².

Taken together, our bioenergetic and proteomic findings allow us to propose a working model of ALS motor neuron metabolic rewiring linking UCP2, HADHA, ACAT2 and HMGCS1 (see Fig. 5D). In this hypothesis, the export of oxaloacetate by UCP2¹⁶ lies at the crossroad between, on the one hand, fatty-acid-supported and TCA cycle-dependent ATP synthesis and, on the other hand, ketogenesis and cholesterol synthesis. The role of UCP2 expression in fatty acid oxidation, ketogenesis and cholesterol synthesis has been suggested in previous studies^{8,45,46}, and our findings support the role of UCP2 in the regulation of cellular ATP levels rather than ROS scavenging. Moreover, HADHA, ACAT2, UCP2 and HMGCS1 are all positively regulated by PPAR α , and a recent study in SODG93A ALS mice showed that PPAR α transcriptional activity is increased in the spinal cord⁴⁷. The fifth protein of interest in our study was isocitrate dehydrogenase isoform 3, which was strongly upregulated in ALS motor neurons (top protein with ACAT2). IDH3 differs from IDH1 and IDH2 in that it reduces NAD⁺, while IDH1 and IDH2 use NADP⁺ as a co-factor. Moreover, IDH1 and IDH2 are reversible and can participate in the reductive carboxylation process involved in *de novo* fatty acid biosynthesis, in contrast with IDH3. Therefore, the overexpression of IDH3 in presymptomatic ALS mouse motor neurons could further facilitate the metabolic shift toward FAO.

The proteomic study of ALS motor neurons revealed significant changes in protein synthesis and degradation, which is in agreement with previous reports showing that altered proteostasis in ALS represents one of the earliest pathological signature of the disease⁴⁸. Proteostasis is a high energy-demanding process, and ER stress alone can activate the upregulation of energy transducing proteins via mTOR inhibition and AMP-activated protein kinase (AMPK) activation⁴⁹. Furthermore, AMPK activation correlates with ALS progression in mutant SOD1 mice motor neurons^{50,51}. Interestingly, reducing AMPK activity pharmacologically or genetically prevents mutant SOD1G93A-induced motor neuron death *in vitro*⁵², suggesting that although AMPK activation promotes energy homeostasis at early stages of neuron differentiation, it could also participate in the onset of progressive neurodegeneration. This view is in accordance with our hypothesis of 'toxic-FAO' in motor neurons, as AMPK stimulates FAO but also promotes ketone body formation and cholesterol synthesis⁵³.

ALS is characterized by the accumulation of protein aggregates that affect the function of motor neurons, and changes in ribosome composition and function might be expected. We found a set of ribosomal proteins and some components of protein processing in the ER that similarly varied in ALS mouse motor neurons and in ALS patients' skin fibroblasts: 40S ribosomal proteins S3, S14, and S23 and 60S ribosomal proteins L8 and L11 were down-regulated, while 78 kDa glucose-regulated protein (HSP5A), dolichyl-diphosphooligosaccharide-protein glycosyltransferase 48 kDa subunit, protein disulfide-isomerase A3 and calreticulin were up-regulated in both models. Those proteins participate in the protein processing module in the ER, which includes components of the ER-associated degradation (ERAD) and components of the unfolded protein response (UPR). In addition to ribosomes and protein processing, we observed a down-regulation of proteins involved in cell adhesion and intercellular contacts in ALS mouse motor neurons. However, little is known about such changes in motor neurons in ALS patients. Recently, Krieger *et al.* questioned the relevance of molecules mediating cell adhesion in the

of oxaloacetate in the TCA on one hand and ketogenesis and cholesterol synthesis on the other. The metabolic alterations observed in ALS patients' skin fibroblasts may not recapitulate what occurs in the spinal cord due to the tissue-specific regulation of energy metabolism⁵⁹. Moreover, All patients cells used in our study were tested for C9ORF72, SOD1, FUS, TDP43 mutations but none of them carried any mutation in these genes. In addition, disease duration could be considered as a potential confounder in the analysis on human skin fibroblasts since most patients were quite long-lived. Most notably, the ALS mouse model used in our study, the SODG93A mutant mice, as well as the patients' skin fibroblasts do not reflect the variety of ALS genetics and pathophysiology. The SOD1G93A mice have additional limitations, as extensively discussed by Philipps and Rothstein⁶⁰.

Finally, our work provides a unique set of data to settle and guide further investigations to define the impact of neurometabolic defects on ALS pathology as well as to propose and evaluate innovative preclinical therapeutic strategies. However, the possibility of exploring whether HADHA, ACAT2 or UCP2 are reliable biomarkers of ALS will require validation studies on a larger number of samples, ideally freshly excised human tissues.

Methods

Chemicals. Reagents were purchased from Sigma, at the exception of the ATP/ADP monitoring kit (Abcam) and the primary antibodies (see the westernblot section below).

Culture of mice motor neurons and patient skin fibroblasts. Motor neurons were obtained from the dissociation of embryonic ventral spinal cords from 12.5 days SOD1-G93A (ALS) and "wild type" control littermate (heterozygous) mice embryos (litters from heterozygous females coupled to homozygous SOD1-G93A males), as described in⁶¹. Briefly, the entire spinal cords were dissected and regrouped by genotype. The dorsal root ganglia and meninges were withdrawn as well as the dorsal part of the spinal cord. The remaining ventral spinal cords were chopped and dissociated with trypsin, and cells were separated by density gradient centrifugation through OptiPrep Density gradient medium. The fractions containing motor neurons were carefully collected and filtered through a BSA cushion, and the purified motor neurons seeded on poly-D-lysine- and laminin-coated culture dishes. Cultures were maintained in Neurobasal medium supplemented with 2% B27, 2% inactivated horse serum, 100 U/ml penicillin and 100 U/ml streptomycin, and with glutamate, glutamine, and neurotrophic factors (GDNF 10 µg/ml, BDNF 1 µg/ml, CTNF 1 µg/ml), in 5% CO₂ at 37 °C. For all the experiments, cells were analyzed between DIV 3 and DIV 5 to ensure minimal glial invasion. The term 'DIV' is widely used in the field of neurosciences when referring to primary neurons in culture and means 'Days *in vitro*'. The method to analyze neuronal cell death after different metabolic treatments was adapted from Szelechowski *et al.*⁶². Briefly, cultures were stained with SMI32 and DAPI and the number of pyknotic nuclei within the SMI32 positive cells were manually assessed on 3 pictures randomly taken for each culture case (20x, open field fluorescence microscope, Leica). At least 100 neurons were analyzed per case and per experiment, on 3 independent experiments.

Primary skin fibroblasts were collected from the arm of ALS patients and control age and gender-matched subjects. All patients were recruited at the reference center for ALS at the hospital of Bordeaux and gave written informed consent to participate in this study, according to the Declaration of Helsinki. The cells were grown in Dulbecco's Modified Eagle Media (DMEM) containing 5 mM glucose and supplemented with 15% fetal bovine serum, 100 U/ml penicillin and 100 U/ml streptomycin, in 5% CO₂ at 37 °C. For all experiments, the cells were harvested during the exponential phase of growth at 70% confluency. The primary fibroblasts cell lines were generated on the same day and the cells underwent the same number of passages (P) at the moment of the various experiments (P4 to P6).

Bioenergetic measurements. Respiration of motor neurons was analyzed on the XF96 analyzer (SeaHorse Biosciences) in XF assay medium while respiration of the skin fibroblasts was evaluated using high-resolution respirometry (Oroboros). The term 'routine' respiration is defined as the respiratory rate of intact cells measured in 5 mM glucose DMEM under atmospheric conditions at 37 °C and sensitive to 2.5 µM antimycin A inhibition. The term 'oligo' respiration is the respiratory rate measured in the routine conditions after addition of the F₁F₀ATP synthase inhibitor oligomycin at 20 µg/ml. This 'oligo' state of respiration does not depend on ADP phosphorylation. The term 'FCCP' respiration defines the rate of respiration measured in the 'oligo' conditions after addition of the uncoupler FCCP used at 2 µM. The 'FCCP' state allows to evaluate the maximal capacity of the respiratory chain in presence of energy substrates and oxygen concentration as defined in the 'routine' conditions. The 'routine/oligo' ratio allows to quantify the coupling degree of the respiratory chain with ADP phosphorylation in the routine conditions. The FCCP/Routine ratio gives a measure of the capacity of the respiratory chain to be chemically uncoupled. It indicates how far from the maximal capacity the routine respiration operates. To assay motor neurons bioenergetics we used the SeaHorse extracellular flux analyzer (XF96). For each run we plated 10.000 cells per well in a 96 well-plate. Each condition was replicated in 3–5 wells (technical replicates) and this experiment was repeated 3 times (biological replicates). The rate of respiration was expressed per 10.000 cells. The primary culture of mouse motor neurons was obtained as follow: typically, one culture dish was obtained from 5 different littermate embryos (pooled). So, the biological replicates correspond to different cultures, each of those obtained from 5 animals.

To assay the ALS patient's derived primary skin fibroblasts we used the Oroboros system. For each run 1 million cells per milliliter of cell culture medium was used. Three technical replicates were performed for three different cultures (biological replicates; N = 3). The rates of respiration were normalized per million of cells. The intracellular ATP content of motor neurons was measured using the bioluminescent ATP determination kit (Molecular Probes, Life Technologies). 20 µL of a cell suspension of 5 × 10⁵ SOD1G93A or wild type motor neurons/mL were plated in a 96-well plate. On DIV 5, cells were treated or not with genipin (20 µM, 45 min), lysed using the lysis buffer provided with the kit (30 µL/well) and the lysates were immediately transferred into

annotated tubes kept in ice and protected from light. ATP concentration was determined by the light-emitting luciferase-catalyzed oxidation of luciferin with ATP and bioluminescence measurement on a luminometer (Luminoskan, Labsystems, Finland). Standardization was performed using known quantities of standard ATP provided with the kit. Determination of the mitochondrial transmembrane electric potential in cultured mice motor neurons was performed by fluorescence imaging using tetramethylrhodamine methyl ester (TMRM). Briefly, cells were incubated with 20 nM TMRM during 20 min. at 37 °C and confocal fluorescence microscopy was performed on a Zeiss Axio Observer microscope equipped with the Vivatome system with a 63x oil spring loaded objective. The images were acquired using AxioVision (6D acquisition and vivatome modules). A minimum of 30 different cells from three different experiments were selected randomly per experimental condition, and the analysis of the fluorescence signal intensity was performed using Morphostryder (Explora Nova).

Mitochondrial morphology analysis. Mitochondria length was measured in all neurites of individualized SOD and WT motor neurons. Mitochondrial network was revealed by Tom20 (mitochondrial outer membrane protein) staining. Mitochondria length was measured and recorded using ImageJ software as described in⁶². For each neuron, mitochondrial tubules were ranked by size categories (short: <2 μM; intermediate: 2–6 μM; long: >6 μM). We analyzed 20 motor neurons per culture, each obtained from 3 to 5 different littermate embryos of each genotype, 3 independent cultures were performed for this analysis.

Proteomics and western blot. The steps of sample preparation and protein digestion, nLC-MS/MS, database search and results processing, and label-free quantitative data analysis were described in⁶³. Briefly, peptide mixture was analyzed on a Ultimate 3000 nanoLC system (Dionex) coupled to a nanospray LTQ-Orbitrap XL mass spectrometer (ThermoFinnigan, San Jose, CA). Data were searched by SEQUEST through Proteome Discoverer 1.4 (Thermo Fisher Scientific Inc.). Raw LC-MS/MS data were imported in Progenesis LC-MS 4.0 (Nonlinear Dynamics Ltd, Newcastle, U.K) and data processing included the following steps: (i) Features detection, (ii) Features alignment across the 12 sample, (iii) Volume integration for 2–6 charge-state ions, (iv) Normalization on total protein abundance, (v) Import of sequence information, (vi) ANOVA test at peptide level and filtering for features $p < 0.05$, (vii) Calculation of protein abundance (sum of the volume of corresponding peptides), (viii) ANOVA test at protein level and filtering for features $p < 0.05$. Noticeably, only non-conflicting features and unique peptides were considered for calculation at protein level. Pathway analysis was performed using IPA (Qiagen), KEGG (String) and Panther. Western blotting was performed as described in⁶³. In this study we used the following Abcam antibodies: SOD1 (ab13498), SOD2 (ab13533) and catalase (ab16731).

ROS production and glutathione REDOX state determination. The cells were trypsinized and counted to obtain a cell suspension of 1×10^6 cells/mL. Changes in cytosolic H_2O_2 levels were monitored using the CM- H_2DCFDA probe. The probe was added to the cell suspension and incubated for 30 min at 37 °C, according to the manufacturer's protocol. The cells were then washed twice in PBS, and fluorescence was measured in a quartz cuvette on a Xenius spectrofluorometer (SAFAS, Monaco, France). A second reading was performed with the addition of 100 μM H_2O_2 in the cuvette to verify the response and absence of saturation of the CM- H_2DCFDA probe. The signal increased immediately after the addition of H_2O_2 in a dose-dependent manner. To evaluate the ratio of GSH/GSSG we used the detection assay kit from Abcam (ab138881) following manufacturer's protocol.

Statistical analysis. All of the data presented in this study correspond to the mean value of n experiments \pm SD, with a minimum of $n \geq 3$. Comparison of the data sets was performed with either the Student's t -test, or the two-way ANOVA test including Sidak's multiple comparison using Prism 7 (Graphpad Software). Two sets of data were considered statistically different when $P < 0.05$. Prior to perform unpaired t test we verified the Gaussian distribution of the data by performing a normality test (Prism 7, GraphPad Software).

Statement. The use of human tissue samples was approved by the University Hospital Center (CHU) of Bordeaux and skin biopsies were obtained at the reference center for ALS at the CHU. Each patient gave written informed consent to participate in this study, according to the Declaration of Helsinki. Moreover, all experiments and methods were carried out in accordance with relevant guidelines and regulations and all experimental protocols were approved by the CHU.

References

- Ghiasi, P., Hosseinkhani, S., Noori, A., Nafissi, S. & Khajeh, K. Mitochondrial complex I deficiency and ATP/ADP ratio in lymphocytes of amyotrophic lateral sclerosis patients. *Neurol. Res.* **34**, 297–303 (2012).
- Israelson, A. *et al.* Misfolded mutant SOD1 directly inhibits VDAC1 conductance in a mouse model of inherited ALS. *Neuron* **67**, 575–587 (2010).
- Peixoto, P. M. *et al.* UCP2 overexpression worsens mitochondrial dysfunction and accelerates disease progression in a mouse model of amyotrophic lateral sclerosis. *Mol. Cell. Neurosci.* **57**, 104–110 (2013).
- Palamiuc, L. *et al.* A metabolic switch toward lipid use in glycolytic muscle is an early pathologic event in a mouse model of amyotrophic lateral sclerosis. *EMBO Mol. Med.* **7**, 526–46 (2015).
- Karbowska, M. & Neutzner, A. Neurodegeneration as a consequence of failed mitochondrial maintenance. *Acta Neuropathol.* <https://doi.org/10.1007/s00401-011-0921-0> (2011).
- Luft, R. *et al.* A case of severe hypermetabolism of non thyroid origin with a defect in the maintenance of mitochondrial respiratory control: a correlated clinical, biochemical and morphological study. *J. Clin. Invest* **41**, 1776–1804 (1962).
- Desquiret, V. *et al.* Dinitrophenol-induced mitochondrial uncoupling *in vivo* triggers respiratory adaptation in HepG2 cells. *Biochim Biophys Acta* **1757**, 21–30 (2006).
- Pequeur, C., Alves-Guerra, C., Ricquier, D. & Bouillaud, F. UCP2, a metabolic sensor coupling glucose oxidation to mitochondrial metabolism? *IUBMB Life* **61**, 762–7 (2009).

9. Pecqueur, C. *et al.* Uncoupling protein 2, *in vivo* distribution, induction upon oxidative stress, and evidence for translational regulation. *J. Biol. Chem.* **276**, 8705–12 (2001).
10. Stuart, J. A., Harper, J. A., Brindle, K. M., Jekabsons, M. B. & Brand, M. D. A mitochondrial uncoupling artifact can be caused by expression of uncoupling protein 1 in yeast. *Biochem. J.* **356**, 779–89 (2001).
11. Harper, J. A. *et al.* Artifactual uncoupling by uncoupling protein 3 in yeast mitochondria at the concentrations found in mouse and rat skeletal-muscle mitochondria. *Biochem. J.* **361**, 49–56 (2002).
12. Couplan, E. *et al.* No Evidence for a Basal, Retinoic, or Superoxide-induced Uncoupling Activity of the Uncoupling Protein 2 Present in Spleen or Lung Mitochondria. *J. Biol. Chem.* **277**, 26268–26275 (2002).
13. Boss, O., Hagen, T. & Lowell, B. B. Uncoupling proteins 2 and 3: potential regulators of mitochondrial energy metabolism. *Diabetes* **49**, 143–56 (2000).
14. Samec, S., Seydoux, J. & Dulloo, A. G. Role of UCP homologues in skeletal muscles and brown adipose tissue: mediators of thermogenesis or regulators of lipids as fuel substrate? *FASEB J.* **12**, 715–24 (1998).
15. Pecqueur, C. *et al.* Uncoupling protein-2 controls proliferation by promoting fatty acid oxidation and limiting glycolysis-derived pyruvate utilization. *FASEB J.* **22**, 9–18 (2008).
16. Voza, A. *et al.* UCP2 transports C4 metabolites out of mitochondria, regulating glucose and glutamine oxidation. *Proc. Natl. Acad. Sci. USA* **111**, 960–5 (2014).
17. Elf, K. *et al.* Alterations in muscle proteome of patients diagnosed with amyotrophic lateral sclerosis. *J. Proteomics* **108**, 55–64 (2014).
18. Lameloise, N., Muzzin, P., Prentki, M. & Assimakopoulos-Jeannet, F. Uncoupling protein 2: a possible link between fatty acid excess and impaired glucose-induced insulin secretion? *Diabetes* **50**, 803–9 (2001).
19. Chevrollier, A., Loiseau, D., Gautier, F., Malthiery, Y. & Stepien, G. ANT2 expression under hypoxic conditions produces opposite cell-cycle behavior in 143B and HepG2 cancer cells. *Mol. Carcinog.* (2004).
20. Pilliod, J. *et al.* New practical definitions for the diagnosis of autosomal recessive spastic ataxia of Charlevoix-Saguenay. *Ann. Neurol.* **78**, 871–86 (2015).
21. Tesson, C. *et al.* Alteration of Fatty-Acid-metabolizing enzymes affects mitochondrial form and function in hereditary spastic paraplegia. *Am. J. Hum. Genet.* **91**, 1051–1064 (2012).
22. Goizet, C. *et al.* REEP1 mutations in SPG31: frequency, mutational spectrum, and potential association with mitochondrial morpho-functional dysfunction. *Hum. Mutat.* **32**, 1118–1127 (2011).
23. Ari, C. *et al.* Metabolic Therapy with Deanna Protocol Supplementation Delays Disease Progression and Extends Survival in Amyotrophic Lateral Sclerosis (ALS) Mouse Model. *PLoS One* **9**, e103526 (2014).
24. Agostini, M. *et al.* Metabolic reprogramming during neuronal differentiation. *Cell Death Differ.* **23**, 1502–1514 (2016).
25. Zheng, X. *et al.* Metabolic reprogramming during neuronal differentiation from aerobic glycolysis to neuronal oxidative phosphorylation. *Elife* **5** (2016).
26. Gascón, S. *et al.* Identification and Successful Negotiation of a Metabolic Checkpoint in Direct Neuronal Reprogramming. *Cell Stem Cell* **18**, 396–409 (2016).
27. Obre, E. & Rossignol, R. Emerging concepts in bioenergetics and cancer research: Metabolic flexibility, coupling, symbiosis, switch, oxidative tumors, metabolic remodeling, signaling and bioenergetic therapy. *Int. J. Biochem. Cell Biol.* <https://doi.org/10.1016/j.biocel.2014.12.008> (2014).
28. Caballero-Hernandez, D. *et al.* The ‘Omics’ of Amyotrophic Lateral Sclerosis. *Trends Mol. Med.* **22**, 53–67 (2016).
29. Benard, G. *et al.* Mitochondrial bioenergetics and structural network organization. *J. Cell Sci.* **120**, 838–848 (2007).
30. Duvezin-Caubet, S. *et al.* Proteolytic processing of OPA1 links mitochondrial dysfunction to alterations in mitochondrial morphology. *J. Biol. Chem.* **281**, 37972–37979 (2006).
31. Lu, J. *et al.* Mitochondrial dysfunction in human TDP-43 transfected NSC34 cell lines and the protective effect of dimethoxy curcumin. *Brain Res. Bull.* **89**, 185–90 (2012).
32. Mühlhling, T., Duda, J., Weishaupt, J. H., Ludolph, A. C. & Liss, B. Elevated mRNA-levels of distinct mitochondrial and plasma membrane Ca(2+) transporters in individual hypoglossal motor neurons of endstage SOD1 transgenic mice. *Front. Cell. Neurosci.* **8**, 353 (2014).
33. Abdel-Khalik, J. *et al.* Defective cholesterol metabolism in amyotrophic lateral sclerosis. *J. Lipid Res.* **58**, 267–278 (2017).
34. Geevasinga, N., Menon, P., Özdinler, P. H., Kiernan, M. C. & Vucic, S. Pathophysiological and diagnostic implications of cortical dysfunction in ALS. *Nat. Rev. Neurol.* **12**, 651–661 (2016).
35. Wiedemann, F. R. *et al.* Impairment of mitochondrial function in skeletal muscle of patients with amyotrophic lateral sclerosis. *J. Neurol. Sci.* **156**, 65–72 (1998).
36. Borthwick, G. M., Johnson, M. A., Ince, P. G., Shaw, P. J. & Turnbull, D. M. Mitochondrial enzyme activity in amyotrophic lateral sclerosis: implications for the role of mitochondria in neuronal cell death. *Ann. Neurol.* **46**, 787–90 (1999).
37. Mattiazzi, M. *et al.* Mutated human SOD1 causes dysfunction of oxidative phosphorylation in mitochondria of transgenic mice. *J. Biol. Chem.* **277**, 29626–33 (2002).
38. Jung, C., Higgins, C. M. J. & Xu, Z. Mitochondrial electron transport chain complex dysfunction in a transgenic mouse model for amyotrophic lateral sclerosis. *J. Neurochem.* **83**, 535–45 (2002).
39. Brown, G. C. The leaks and slips of bioenergetic membranes. *FASEB J.* **6**, 2961–5 (1992).
40. Rottenberg, H. Decoupling of oxidative phosphorylation and photophosphorylation. *Biochim. Biophys. Acta* 1018–1 (1990).
41. Shephard, S. R. *et al.* Urinary p75^{ECD}. *Neurology* **88**, 1137–1143 (2017).
42. Ebert, D., Haller, R. G. & Walton, M. E. Energy contribution of octanoate to intact rat brain metabolism measured by ¹³C nuclear magnetic resonance spectroscopy. *J. Neurosci.* **23**, 5928–35 (2003).
43. Cacabelos, D. *et al.* Interplay between TDP-43 and docosahexaenoic acid-related processes in amyotrophic lateral sclerosis. *Neurobiol. Dis.* **88**, 148–60 (2016).
44. Luan, H. *et al.* LC-MS-based urinary metabolite signatures in idiopathic Parkinson’s disease. *J. Proteome Res.* **14**, 467–78 (2015).
45. Nakatani, T., Tsuboyama-Kasaoka, N., Takahashi, M., Miura, S. & Ezaki, O. Mechanism for peroxisome proliferator-activated receptor- α activator-induced up-regulation of UCP2 mRNA in rodent hepatocytes. *J. Biol. Chem.* **277**, 9562–9 (2002).
46. Lee, S. S. T. *et al.* Requirement of PPAR α in maintaining phospholipid and triacylglycerol homeostasis during energy deprivation. *J. Lipid Res.* **45**, 2025–37 (2004).
47. Qi, Y. *et al.* Differential peroxisome proliferator activated receptors activity in a rodent model of amyotrophic lateral sclerosis. *Int. J. Clin. Exp. Med.* **8**, 3743–51 (2015).
48. Rozas, P., Bargsted, L., Martínez, F., Hetz, C. & Medinas, D. B. The ER proteostasis network in ALS: Determining the differential motoneuron vulnerability. *Neurosci. Lett.* <https://doi.org/10.1016/j.neulet.2016.04.066> (2016).
49. Kemter, E., Fröhlich, T., Arnold, G. J., Wolf, E. & Wanke, R. Mitochondrial Dysregulation Secondary to Endoplasmic Reticulum Stress in Autosomal Dominant Tubulointerstitial Kidney Disease - UMOD (ADTKD-UMOD). *Sci. Rep.* **7**, 42970 (2017).
50. Perera, N. D. *et al.* Mutant TDP-43 Deregulates AMPK Activation by PP2A in ALS Models. *PLoS One* **9**, e90449 (2014).
51. Coughlan, K. S., Mitchem, M. R., Hogg, M. C. & Prehn, J. H. M. ‘Preconditioning’ with latrepirdine, an adenosine 5'-monophosphate-activated protein kinase activator, delays amyotrophic lateral sclerosis progression in SOD1G93A mice. *Neurobiol. Aging* **36**, 1140–1150 (2015).
52. Lim, M. A. *et al.* Reduced Activity of AMP-Activated Protein Kinase Protects against Genetic Models of Motor Neuron Disease. *J. Neurosci.* **32**, 1123–1141 (2012).

53. Blázquez, C., Woods, A., de Ceballos, M. L., Carling, D. & Guzmán, M. The AMP-activated protein kinase is involved in the regulation of ketone body production by astrocytes. *J. Neurochem.* **73**, 1674–82 (1999).
54. Krieger, C., Wang, S. J. H., Yoo, S. H. & Harden, N. Adducin at the Neuromuscular Junction in Amyotrophic Lateral Sclerosis: Hanging on for DearLife. *Front. Cell. Neurosci.* **10** (2016).
55. Matthews, R. T., Yang, L., Browne, S., Baik, M. & Beal, M. F. Coenzyme Q10 administration increases brain mitochondrial concentrations and exerts neuroprotective effects. *Proc. Natl. Acad. Sci. USA* **95**, 8892–7 (1998).
56. Shefner, J. M. *et al.* A clinical trial of creatine in ALS. *Neurology* **63**, 1656–61 (2004).
57. Bouzier-Sore, A.-K., Serres, S., Canioni, P. & Merle, M. Lactate involvement in neuron-glia metabolic interaction: (13)C-NMR spectroscopy contribution. *Biochimie* **85**, 841–8 (2003).
58. Jose, C., Melser, S., Benard, G. & Rossignol, R. Mitoplasticity: Adaptation Biology of the Mitochondrion to the Cellular Redox State in Physiology and Carcinogenesis. *Antioxid. Redox Signal.* **18**, 808–849 (2013).
59. Benard, G. *et al.* Physiological diversity of mitochondrial oxidative phosphorylation. *Am J Physiol Cell Physiol* **291**, C1172–82 (2006).
60. Philips, T. & Rothstein, J. D. Rodent Models of Amyotrophic Lateral Sclerosis. *Curr. Protoc. Pharmacol.* **69**, 5.67.1–21 (2015).
61. Henderson, C., Bloch-Gallego, E. & Camu, W. In *Neural Cell Culture, A Practical Approach* (eds Cohen, J. & Wilkin, G.) (Oxford University Press, 1995).
62. Szelechowski, M. *et al.* A viral peptide that targets mitochondria protects against neuronal degeneration in models of Parkinson's disease. *Nat. Commun.* **5**, 5181 (2014).
63. Imasawa, T. *et al.* High glucose repatterns human podocyte energy metabolism during differentiation and diabetic nephropathy. *FASEB J.* <https://doi.org/10.1096/fj.201600293R> (2016).

Acknowledgements

The authors would like to thank Pierre Costet from the animal facility of the University of Bordeaux for valuable assistance. We also acknowledge Dr. Giuseppe Fiermonte for scientific discussions. Lastly, we thank the funding organizations which supported this work: Association Française contre les Myopathies – Téléthon (AFM-Téléthon; Grant ‘Savenerg’), Agence Nationale pour la Recherche (ANR; grant COSMIT 2015-0451), Brazilian National Counsel of Technological and Scientific Development (CnPQ), CAPES-COFECUB, CELLOMET and INSERM.

Author Contributions

S.M., A.N., O.E., and A.L. performed the experiments of bioenergetics and cell biology. L.C. performed motor neurons preparation and cell culture. B.M. and C.S. performed the mass spectrometry proteomic experiments. L.D., O.S., and C.S. participated to data analysis and scientific discussions. L.M.G. and R.R. designed the study, analyzed the data and wrote the manuscript.

Additional Information

Supplementary information accompanies this paper at <https://doi.org/10.1038/s41598-018-22318-5>.

Competing Interests: The authors declare no competing interests.

Publisher's note: Springer Nature remains neutral with regard to jurisdictional claims in published maps and institutional affiliations.



Open Access This article is licensed under a Creative Commons Attribution 4.0 International License, which permits use, sharing, adaptation, distribution and reproduction in any medium or format, as long as you give appropriate credit to the original author(s) and the source, provide a link to the Creative Commons license, and indicate if changes were made. The images or other third party material in this article are included in the article's Creative Commons license, unless indicated otherwise in a credit line to the material. If material is not included in the article's Creative Commons license and your intended use is not permitted by statutory regulation or exceeds the permitted use, you will need to obtain permission directly from the copyright holder. To view a copy of this license, visit <http://creativecommons.org/licenses/by/4.0/>.

© The Author(s) 2018